Asian Journal of Medicine and Health

19(4): 56-69, 2021; Article no.AJMAH.68757
ISSN: 2456-8414

Radiographic Anatomy of the Canine Appendicular Skeleton

Kabkia Dieudoné[1]*, Kadja Mireille[1], Gbande Pihou[2], Sonhaye Lantam[2] and Agba Kondi[3]

[1]Ecole Inter-Etats des Sciences et Médecine Vétérinaires (EISMV) (Dakar, Sénégal), Senegal.
[2]Faculté des Sciences de la Santé, Université de Lomé, (Lomé, TOGO), Senegal.
[3]Université de Lomé, Ecole Supérieure d'Agronomie (Lomé, TOGO), Senegal.

Authors' contributions

This work was carried out in collaboration among all authors. Author KD conducted the study, wrote the protocol, took the radiographic images and wrote the first version of the manuscript under the direction of authors KM, GP, SL, AK, who made their corrections for the validation of the final document submitted. All authors read and approved the final manuscript.

Article Information

DOI: 10.9734/AJMAH/2021/v19i430322
Editor(s):
(1) Dr. P. Veera Muthumari, V. V. Vanniaperumal College for Women, India.
Reviewers:
(1) Jasvinder Singh Sasan, SKUAST-J, India.
(2) Snehangsu Sinha, College of Veterinary Science, India.
Complete Peer review History: http://www.sdiarticle4.com/review-history/68757

Original Research Article

Received 18 March 2021
Accepted 23 May 2021
Published 27 May 2021

ABSTRACT

Objectives: Being the most common pet in Africa, the dog is often subject to various diseases, especially appendicular. A good knowledge of the normal radiographic anatomy is an important support for the clinician for the interpretation of radiographic pictures of the appendicular skeleton. The aim of this study was to produce a radio-anatomical atlas of the appendicular skeleton of the dog in order to facilitate the understanding and interpretation of radiographic images of the dog.
Methodology: For this purpose, radiographs were performed on all regions of the limbs of healthy dogs received at the radiology room.
Results: At the end of the study, the best normal radiographs by anatomical region and by incidence of normal limb radiographs, were selected constituting a reference database of radiographic anatomy of this animal. Each radiograph is commented and annotated, facilitating the understanding of the pictures.

**Corresponding author: E-mail: dieudone.kabkia@yahoo.com;*

Conclusion: These radiographs will serve as a basis for the interpretation of radiographic images of the appendicular skeleton in the dog.
Decrease medical as well as financial burden, hence improving the management of cirrhotic patients. These predictors, however, need further work to validate reliability.

Keywords: Anatomy; appendicular; canine; radiography; skeleton.

1. INTRODUCTION

Radiography is the fixation of three-dimensional structures projected by a beam of incident X-rays on a flat support. These X-rays interact with a photosensitive emulsion deposited on the radiographic film and this interaction will be made visible by the development of the film. Thus, any non-ideal projection will give a distorted image of the real object. Radiography, discovered in 1985 by Wilhem Conrad RONTGEN, is currently of great diagnostic interest in many fields of medicine. Indeed, radiography is a complementary examination, which allows to confirm or invalidate a clinically established diagnosis. In animals, as in humans, radiographs provide precise information on the anatomy of many organs, its topography and morphology and its relationship with surrounding tissues, and on the evolution of a treatment in progress [1]. It is thus used for the diagnosis of diseases of the animal's body, especially of the limbs (for the search for fractures but also for the evaluation of various joint problems such as osteoarthritis or dysplasia for example).

In addition, carnivores, especially dogs, are the animals most concerned by this complementary examination, and they are the species most frequently requested for radiography during consultations in private practices in Dakar [2,3] and at the EISMV clinic. Facilitating the diagnostic and therapeutic process, radiography is a first-line complementary examination in many diseases of the dog, whether medical or orthopedic in nature. Although radiography is a very accessible examination in practice, the interpretation of the images obtained requires a good knowledge of the anatomy, as well as of the normal radiographic aspect, for a given species. Therefore, the purpose of this study is to describe the radiographic anatomy of the appendicular skeleton of the dog in order to facilitate the understanding and interpretation of radiographic images of the dog and to be a significant aid in the interpretation of our patients' images.

2. MATERIALS AND METHODS

2.1 Area, Period of Study

The veterinary clinic of the EISMV of Dakar is located within the establishment at the University Cheikh Anta Diop (U.C.A.D) of Dakar in the Fann district. It is a referral clinic that is currently one of the most frequented veterinary clinics in the city of Dakar due to the quality of the services offered to patients. This study took place from June 2018 to August 2019.

2.2 Materials

2.2.1 Animal material

To conduct this study, we used unanesthetized dogs, regardless of weight, age, and height. These were dogs presented to the radiology room for routine radiography and whose owners had agreed to their participation in the study. Dogs were recruited as they arrived in the radiology room. We thus recruited a total of 30 patients. The animals were healthy animals, referred by clinicians at the EISMV University Hospital and also by clinical veterinarians in private practice for routine examinations, and brought by the animal owners.

2.2.2 Radiographic equipment

The Inter-State School of Veterinary Sciences and Medicine of Dakar has a radiology room in the clinic where the present study was conducted. The radiographic apparatus used is of the brand CAWOWAT. This device has the following characteristics:

- Maximum voltage (kV): 150 kV
- Maximum second milliamperage: 300 mAs

The adjustment of these parameters is done thanks to the control panel of the radiographic apparatus.

2.3 Methods

2.3.1.Animal restraint

We did not need any physical or medicinal restraint. Our animals were brought by their

owners, which allowed us to carry out the manipulations in complete tranquillity. The presence of the owners was a reassuring factor, avoiding the need for physical and medicinal restraint.

2.3.2 Technique for performing the radiography of the appendicular skeleton

The radiographic examination of the appendicular skeleton is centered either on the bony shafts or on the joints. When radiographing a whole bone, it was necessary to obtain at least two orthogonal projections. The proximal and distal joints must be included in the image (Figs 1 and 2). When radiographing a joint, a bony portion on either side of the joint should be included in the image if possible. When taking the image, it is important to ensure that the bone or joint structure to be radiographed is as close as possible to the cassette in order to avoid geometric blurring [4,5,6].

2.3.3 Position of the animal

For lateral exposure, the dog was laid in dorsal recumbency and the limb to be radiographed was in extension. In ventro-dorsal incidence, the limb to be radiographed, against the table, is brought forward in extension [4,5,6].

2.3.3 Quality criteria

The centering must be exactly on the joint and the distal and proximal third of the bones must be visible [4,5,6].

Fig. 1. Cranio-caudal incision of the limb (Photo KABKIA)

Fig. 2 Lateral incidence of the limb (Photo KABKIA)

The skull is a complex structure to study in radiography. Indeed, the number of bones and the resulting superimpositions make it difficult to use the images obtained (Figs 1 and 2). A standard examination of the skull must be performed by taking two radiographic images with orthogonal incidences [4,5,6].

2.3.4 Selection and obtaining of the images included in the thesis

The best images were chosen by assessing the incidence, position and quality criteria stated in our methodology for taking radiological images [4,5,6].

The different images were placed on the view box and pictures were taken with the digital camera. In addition, for each image, arrows were used to annotate the characteristic anatomical elements in order to facilitate the understanding of the images. Finally, with the Windows Screen Capture and Sketch Tool software, the arrowed and numbered images were captured in order to avoid moving the arrows.

3. RESULTS AND DISCUSSION

3.1 Results

3.1.1 Thoracic limb

3.1.1.1 Shoulder joint

Caudocranial incidence (Fig. 3)

The scapula is clearly visible with the supraspinous fossa and the infraspinous fossa. the scapular spine forms a more prominent radiodensity line and extends to the neck of the scapula to form the acromion. The distal end of the scapula is wide and the supraglenoid tubercle is visible cranially. The joint is formed by the glenoidal cavity where the head of the humerus is housed. On the image, the contours of the humeral head are clearly visible as well as the major tubercle.

Mediolateral view (Fig. 4)

On this projection, the supraglenoidal tubercle of the scapula, the insertion site of the biceps brachii muscle, is clearly visible. The humeral head, clearly visible and hemispherical in shape, articulates with the glenoidal cavity of the scapula. Its caudal edge was be smooth and regular in outline and the subchondral bone should be homogeneously opaque. Laterally, the major tubercle of the humerus was clearly visible.

3.1.1.2 Elbow joint

Cranio-caudal view (Fig. 5)

On this projection, both parts of the humeral condyle are clearly visible. The capitulum is located laterally and the trochlea medially. The two epicondyles are also clearly visible. The supra-condylar foramen and the olecranon fossa of the humerus are superimposed on the olecranon.

Mediolateral Incidence (Fig. 6)

The elbow is a complex region with three bones: the humerus, radius, and ulna. The humero-ulnar, humero-radial and radio-ulnar joint spaces are narrow and regular. However, in the middle part of the humero-ulnar joint space, it is possible to observe a discrete widening that corresponds to the synovial fossa of the ulna.

The medial epicondyle of the humerus is clearly visible and faces the coronoid process of the radius and the trochlear incision of the ulna. These structures are highlighted by a more marked radiodensity. On this projection, we also clearly distinguish the anconeal process of the ulna and the tuberosity of the olecranon.

3.1.1.3 Carpus, metacarpus and phalanges

Dorso-palmar view (Fig. 7)

It is difficult to obtain good definition images of the dog's hand because of the small size of this region and the thinness of the bony structures that compose it.

Because it is composed of seven small bones, the carpus is a difficult area to study radiographically. Indeed, in addition to the fineness and spatial complexity of this bony structure, the carpus is very short because of the plantigrade. Under this dorsopalmar incidence, the distinction between the different carpal bones is difficult. Nevertheless, the projection of the pisiform bone or accessory bone of the carpus can be distinguished medially and appears with a more marked radiodensity. It is very developed in the dog because of the plantigrade. In fact, it receives the termination of the ulnar flexor carpus and ulnar extensor carpus muscles.

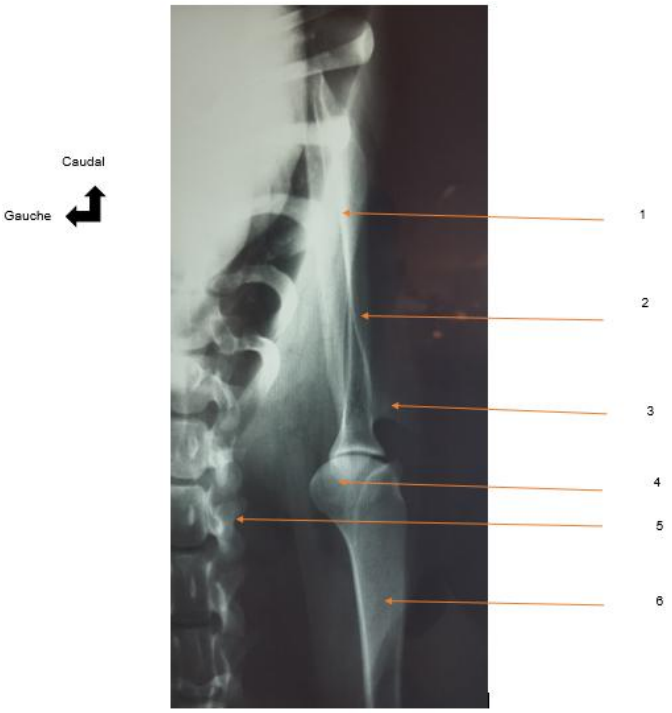

Fig. 3. Radiograph of the shoulder joint in left cranio-caudal view (Photo KABKIA)
1= Scapula; 2= Scapular spine; 3 = Acromion; 4 = Minor tubercle; 5 = Cervical vertebrae; 6 = Humerus

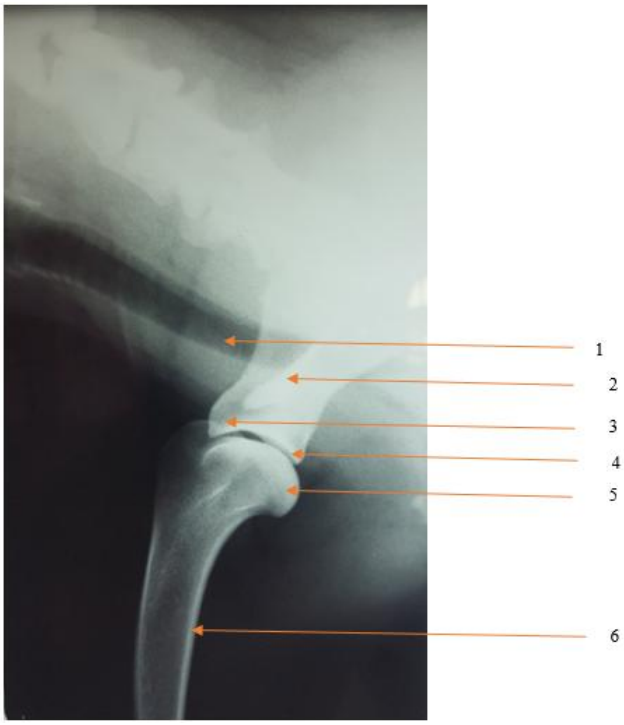

Fig. 4. Radiograph of the shoulder joint in left medial-lateral view (Photo KABKIA)
1= Trachea; 2= Acromion; 3 = Supraglenoid tubercle; 4 = Infraglenoid tubercle; 5 = Femoral head; 6 = Humerus

Fig. 5. X-ray of the elbow joint in left craniocaudal view (Photo KABKIA)
1= Humerus; 2= Lateral epicondyle; 3 = Olecranon; 4 = Medial epicondyle; 5 = Ulna; 6 = Radius

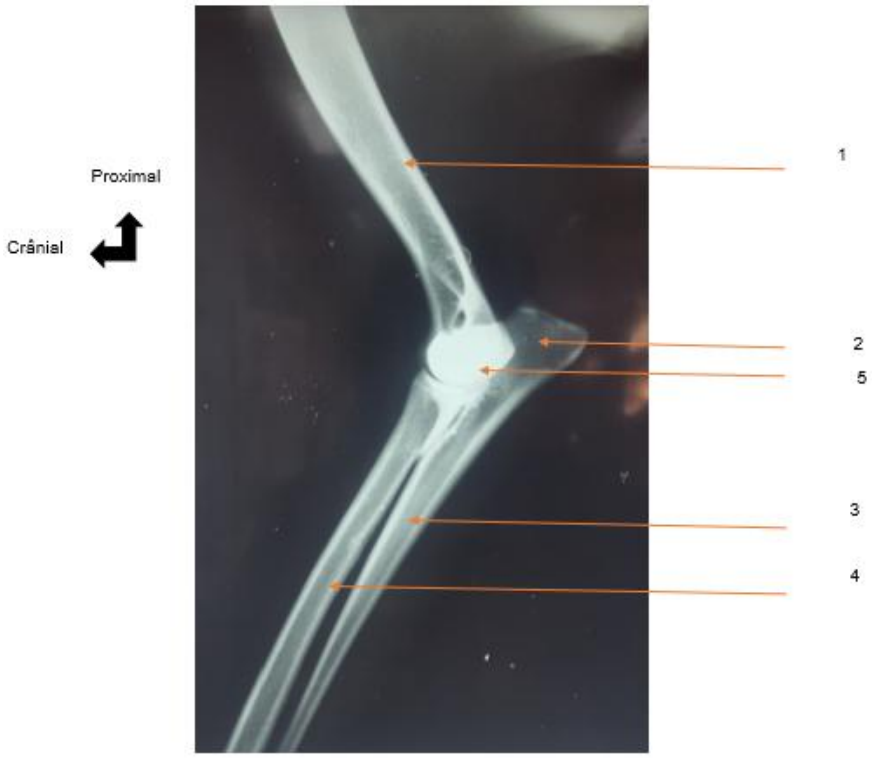

Fig. 6. Radiograph of the elbow in medio-lateral incidence (Photo KABKIA)
1= Humerus; 2= Olecranon; 3 = Ulna; 4 = Radius; 5 = Humeral trochlea

The metacarpus is made of five metacarpal bones arranged parallel to each other. They are numbered from I to V from medial to lateral. Each of these bones responds by its proximal end to one of the parts of the distal row of the carpus and by its distal end to a phalanx. We note that metacarpal bones III and IV are the longest. Each metacarpophalangeal joint has two small sesamoid bones on the palmar side.

The fingers of the hand are composed of three phalanges, except for finger I which has only two. Each of the distal phalanges has a well-developed claw that can be seen on x-ray.

Mediolateral Incidence (Fig. 8)

In larger animals, this projection allows the two rows of carpal bones to be observed correctly, which is practically impossible in the dog. Nevertheless, the pisiform bone is clearly visible because it is projected along its long axis. The metacarpal bones and phalanges are superimposed on this projection, and therefore difficult to evaluate.

3.1.2 Pelvic limb

3.1.2.1 Pelvis - Hip joint

Lateral Incidence (Fig. 9)

We observe the ilium cranially. Dorsally, we distinguish the iliac crest. In the dog, the ventro-cranial iliac spine (or hip angle) is flattened. The neck of the ilium is poorly marked. Progressing caudally, we observe dorsally the large sciatic notch. The ischial tuberosity can be seen caudo-dorsally.

The table of the pubic bone is wide and rectangular, while the pubic ramus is small. On this projection, the obturated hole appears ovoid in shape.

Dorso-ventral view (Fig. 10)

The pelvis is formed by the union of the two coxal bones at the pubic symphysis. Each coxal bone is made up of three bones, the ilium, the ischium and the pubis, which converge and unite on the acetabulum to support the femur. The ilium is thin. The ventrocaudal iliac spine (or hip angle) and the body of the ilium are aligned. Cranially, the wing of the ilium meets the sacrum to form the sacroiliac joint. The obturated foramen, which appears on this triangular-shaped projection, is large. It is bounded cranially by the cranial branch of the pubis, laterally and ventrally by the ischium. Laterally to the sciatic spine, we distinguish the edge of the acetabulum. This projection allows us to evaluate the hip joints. The femoral heads are spherical, with a smooth and regular contour and homogeneous opacity.

3.1.2.2 Stifle joint

Cranio-caudal view (Fig. 11)

The stifle joint consists of several bony elements: the femur, patella, tibia, and fibula. Cranially, the patella fits into the femoral trochlea to form the patellofemoral joint. The distal end of the femur articulates with the tibial plateau via the femoral condyles, the projections of which overlap under this radiographic incidence.

They have a smooth and regular contour and a homogeneous opacity. The head of the fibula projects onto the caudal part of the proximal epiphysis of the tibia.

Mediolateral view (Fig. 12)

On this projection, we observe that the medial femoral condyle is wider than the lateral femoral condyle. We can see the projection of the patella, which is superimposed on the femoral trochlea. The intercondylar eminence, carried by the tibial plateau between the two condyles, corresponds to the intercondylar fossa of the femur.

The femoral-tibial joint space is fairly well projected at this angle. An impression of joint collapse often exists, but it is due to the non-tangential projection of the joint space.

3.1.2.3 Tarsus

Dorso-plantar incidence (Fig. 13)

In the dog, the tarsus is wider than the carpus. Nevertheless, obtaining a good quality image of this region remains difficult because of the thinness of the bony structures that compose it and its radiographic study is complex.

On this image, we can see the projection of the calcaneus, which is the longest bone of the tarsus. It has an articular surface for the fibular malleolus and another for the central tarsal bone.

Fig. 7. Radiograph of the carpus, metacarpus and phalanx in left dorso-plantar incidence (Photo KABKIA)

1= Carpus; 2 = Metacarpus; 3 = Proximal phalanx; 4= Middle phalanx; 5 = Distal phalanx

Fig. 8. Radiograph of the carpus, metacarpus, phalanges in left medio-lateral incidence (Photo KABKIA)

1= Ulna; 2= Radius; 3 = Pisiform bone; 4 = Metacarpals; 5 = Greater sesamoid; 6 = Proximal phalanx; 7 = Middle phalanx; 8 = Distal phalanx

Fig. 9. X-ray of the pelvis in left dorso-ventral incidence (Photo KABKIA)
1= Ilium; 2= Caudal vertebrae; 3 = Acetabulum; 4 =Pubis; 5 = Femoral head; 6 = Ischium; 7 = Femur

Fig. 10. Radiograph of the pelvis in left lateral incidence (Photo KABKIA)
1= Caudal vertebrae; 2= Ilium; 3 = Sacrum; 4 = Ischium; 5 = Femoral head; 6 = Oval hole

Fig. 11. Radiograph of the stifle joint in left cranial-caudal view (Photo KABKIA)
1= Femur ; 2= Patella ; 3 = Tibial plateau; 4 = Fibula; 5 = Tibia

Fig. 12. Radiograph of the stifle joint in left medial-lateral view (Photo KABKIA)
1= Femur; 2= Patella; 3 = Femoral condyle; 4 = Tibial plateau; 5 = Tibia

Together with the calcaneus, the talus forms the proximal row of tarsal bones. Located medially, it articulates with the tibial malleolus on the one hand and with the central tarsal bone on the other.

The distal tarsal row is composed of the tarsal bones numbered I to IV from the tibial side to the fibular side. As in all mammals, the tarsal bone IV results from the fusion of the tarsal bones IV and V. They articulate distally with the metatarsal bones. The central tarsal bone articulates with the talus and helps form the tarsal canal.

Mediolateral Incidence (Fig. 14)

The two trochleae of the talus must be superimposed. On this projection, the superposition of the bones that make up the tarsus makes the interpretation of the image complex. The tuberosity of the calcaneus, the bony base of the point of the hock and the termination point of the gastrocnemius muscle, is clearly visible.

3.1.2.4 Metatarsus

Dorso-plantar incidence (Fig. 13)

There is a similarity in construction between the skeletons of the hand and the foot. However, the metatarsal bones and phalanges of the foot are longer than the metacarpal bones and phalanges of the hand.

The metatarsal is made up of five metatarsal bones arranged parallel to each other. Each of these long bones has its proximal end connected to one of the pieces of the distal tarsal row and its distal end to a finger. Each metatarsal bone bears two small sesamoid bones on its distal part. Note that metatarsal bone I is shorter and metatarsal bones III and IV are the longest.

The toes of the foot have, like those of the hand, three phalanges each, except the first one which has only two. Each of the distal phalanges has a well developed claw in the dog.

Medio-lateral incidence (Fig. 14)

We note a superposition of the two trochleae of the talus. On this projection, the metatarsal bones and phalanges are more or less superimposed and therefore difficult to evaluate. We can nevertheless correctly distinguish the metatarsal bone I and the two phalanges of finger I.

3.2 Discussion

We worked on the local breed dog which represents the animal species most frequently brought in for this complementary examination, the radiography. Indeed, the canine species accounts for nearly 75% of the complementary examinations performed in clinics in the Dakar region. This high frequency can be explained by the fact that the canine species has an inestimable emotional value for its owner in addition to its usefulness in the daily life of its master. In addition, 54.55% of the clinics in Dakar with a canine specialty use complementary examinations and radiology constitutes 62.5% of the analyses requested by them. This can be explained by the fact that radiography has the advantage of being more accessible. [7].

Our study focused on the radiographic anatomy of the appendicular skeleton of the dog because appendicular skeletal disorders are among the most frequent disorders in dogs in Dakar. Our method of interpretation of X-ray pictures of the appendicular skeleton of the dog was the same as that used by GASSE in 2008, LEBAS in 2008, SCHEVENEMENT in 2010, and CHATOR, 2010 who had to work respectively on the chinchilla, ferret, dog and red fox [7,8,9]. This interpretation method is based on the appreciation of density, contrast, sharpness, position and centering and framing. However, a different method of interpretation of radiological images was used by GATTI in 2006 in horses [10]. Indeed, for each horse and each radiographic workup, any original, suspicious or abnormal image is noted on a summary sheet detailing all potential osteoarticular lesion sites. Each image is characterized and graded and these grades correspond to a number of points, directly dependent on their severity. The sum of all the points of each horse allows to establish its osteoarticular status. It should be noted that, in general, the interpretation of radiographic images is much easier with digital radiography and the images obtained with digital radiography are of as good, if not better, quality than with silver radiography. In fact, with film radiography, the operator must sometimes choose between the quality of the contrast and the detail of the spatial resolution. Digital radiography offers a much larger scale of gray levels for each pixel of the sensor. This makes it possible to detect minimal

differences between the X-rays arriving on the sensor, the contrast is increased and a slight under or overexposure may not hinder the interpretation of the image which can be reworked by the software. This feature has two advantages. It is much rarer than in conventional radiography to have to repeat the image. Moreover, on the same image, it becomes possible to study very different tissues (such as soft tissue and bone for example). Associated with this gain in contrast, the number of pixels theoretically limits the spatial resolution, which becomes less good than on high quality films. However, the spatial resolution is still better than what the human eye is able to detect. Digital technology also offers the advantage of being able to annotate images and make measurements while keeping a copy of the original image.

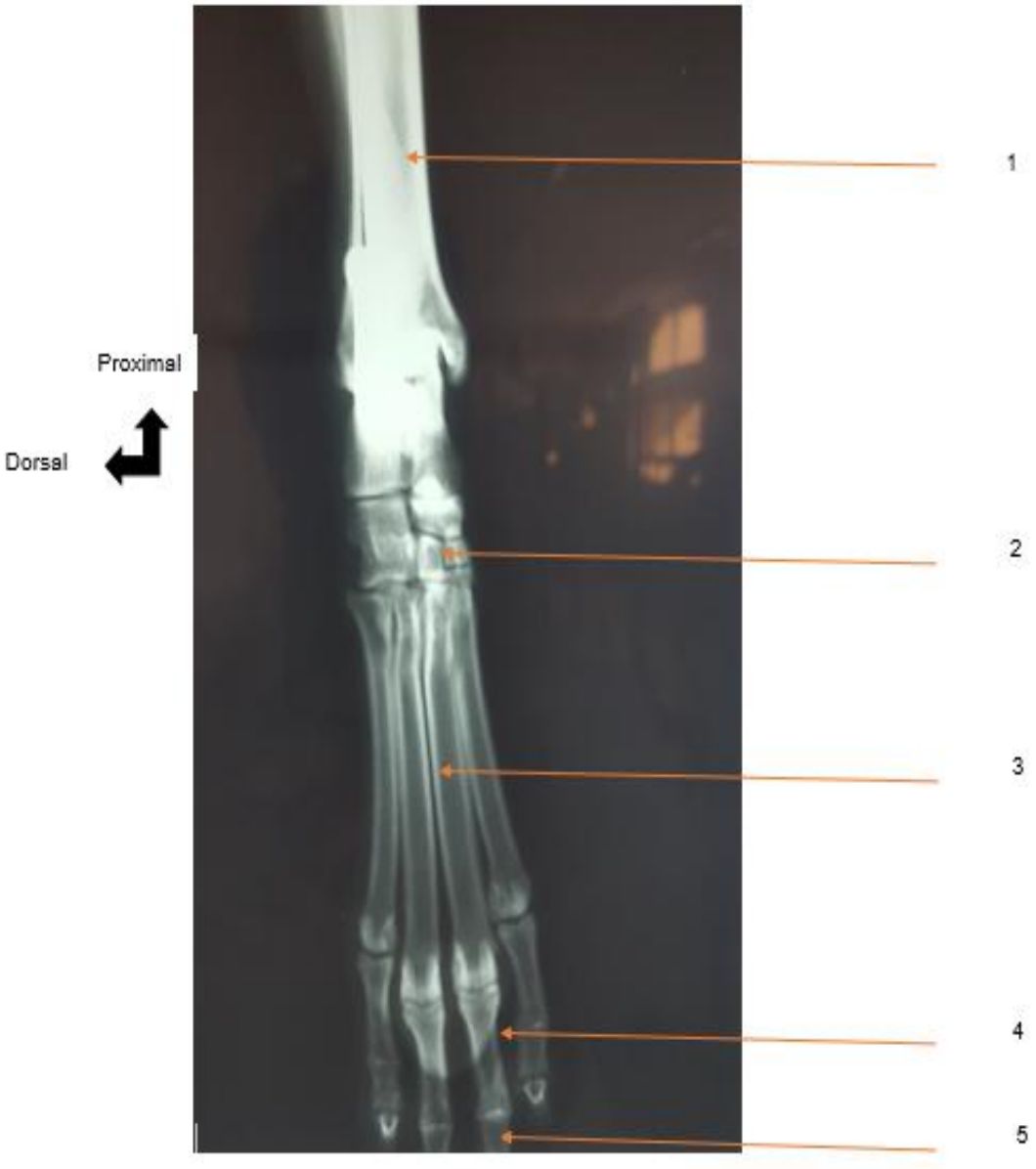

Fig. 13. Radiograph of the tarsus, metatarsus, phalanges in left dorso-plantar incidence (Photo KABKIA)

1= Tibia; 2= Tarsus; 3= Metatarsus; 4= Proximal phalanx; 5= Middle phalanx

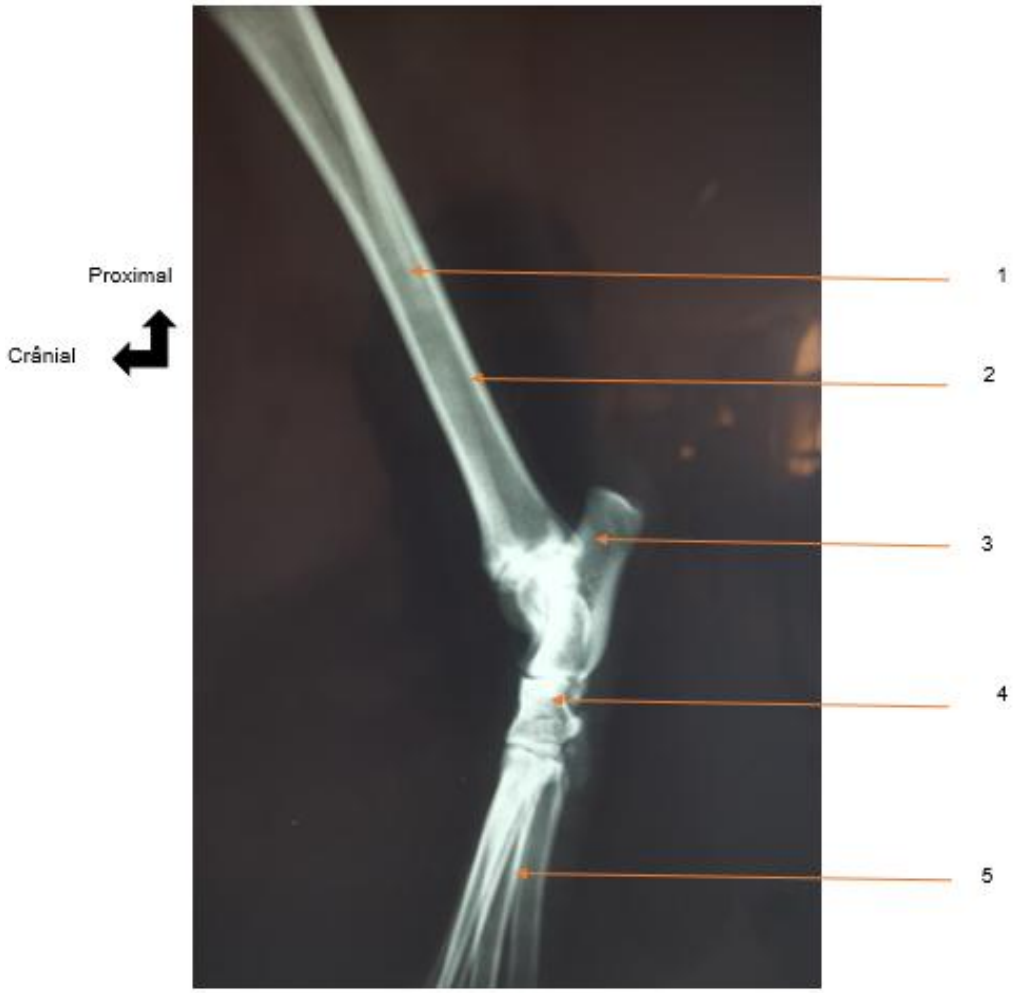

Fig. 14. Radiograph of the tarsus, metatarsus in left medial-lateral incidence (Photo KABKIA)
1= Fibula ; 2= Tibia ; 3 = Calcaneus ; 4 = Tarsus ; 5 = Metatarsus

4. CONCLUSION

The objective of this study was to describe the radiographic anatomy of the dog's limbs in order to facilitate the understanding and interpretation of radiographic images of the dog's axial skeleton. At the end of our study, we obtained radiographic images that were annotated and that will serve as a basis for the interpretation of radiographic images of this important anatomical region.

CONSENT

It is not applicable.

ETHICAL APPROVAL

Animal Ethic committee approval has been taken to carry out this study.

COMPETING INTERESTS

Authors have declared that no competing interests exist.

REFERENCES

1. Solacroup B, et Le Marec SC. Bases physiques des rayons X, CERF, French. 2001;21.
2. Fossog Tine FX. Evaluation de la demande et du cout des analyses complémentaires dans les cliniques vétérinaires privées de la région de Dakar, Thèse : Med. Vet : Dakar, French; 2008.
3. Kouakou Deassath HB. Etude rétrospective des cas cliniques de carnivores domestiques vus en

consultation médicale a l'EISMV de Dakar de 2005 à 2010, Thèse : Med. Vet : Dakar, French; 2010.

4. Barthez, P. Technique en radiologie des petits animaux. Paris: CNVSPA-PMCAC, French. 1997;180.
5. Chator O. Atlas radiographique du renard roux (Vulpes vulpes), Thèse: Med. Vet : Toulouse, French; 2010.
6. MAÏ W. Guide pratique de radiographie canine et féline. Paris: Editions MED'COM, French. 2003;350.
7. Kouakou Deassath HB. Etude rétrospective des cas cliniques de carnivores domestiques vus en consultation médicale a l'EISMV de Dakar de 2005 à 2010, Thèse : Med. Vet : Dakar, French; 2010.
8. Gasse S. Contribution radiologique et ostéologique à la connaissance du Chinchilla (Chinchilla lanigera), Thèse : Med. Vet : Toulouse, French; 2008.
9. Van Heesewijk HP, Van Der Graaf Y, De Valois JC, Vos JA, Feldberg MAM. Chest imaging with a selenium detector versus conventional film radiography: A CT-controlled study. Radiology 1996;200:687-90.
10. Gatti J. Evolution radiographique des membres (pieds exceptés) de soixante deux chevaux entre trois et seize ans. Thèse: Med. Vet : Alfort; 2006.

Peer-review history:
The peer review history for this paper can be accessed here:
http://www.sdiarticle4.com/review-history/68757